Supplementary material for

Intercomparison of global foliar trait maps reveals fundamental differences and limitations of upscaling approaches

Benjamin Dechant[1,2], Jens Kattge[3,1], Ryan Pavlick[4], Fabian D. Schneider[4], Francesco M. Sabatini[5,6], Alvaro Moreno-Martinez[7], Ethan E. Butler[8], Peter M. van Bodegom[9], Helena Vallicrosa[10,11,12], Teja Kattenborn[13,1], Coline C.F. Boonman[14], Nima Madani[15,4], Ian J. Wright[16,17], Ning Dong[18,19], Hannes Feilhauer[20,1], Josep Penuelas[11,12], Jordi Sardans[11,12], Jesus Aguirre-Gutierrez[21,22], Peter B. Reich[23,8,16] Pedro J. Leitão[20,1], Jeannine Cavender-Bares[24], Isla H. Myers-Smith[25], Sandra M. Duran[26], Holly Croft[27], I. Colin Prentice[18,28], Andreas Huth[29,30,1], Karin Rebel[31], Sönke Zaehle[3], Irena Simova[32,33], Sandra Diaz[34,35], Markus Reichstein[3,1], Christopher Schiller[36], Helge Bruelheide[37,1], Miguel Mahecha[20,1], Christian Wirth[38,3], Yadvinder Malhi[21,22], Philip A. Townsend[4,39]

Remote Sensing of Environment

Part 1

Additional information on **existing upscaled maps**

Table S1: Full list of predictor variables used in global trait upscaling. Note that only the predictors of the final models are shown here and in case of VC predictors that were selected at least twice among the different PFT categories and N and P upscaling are shown. Abbreviations for the trait products are BG: van Bodegom, BL: Butler, BM: Boonman, MD: Madani, MM: Moreno, SL: Schiller, VC: Vallicrosa.

Predictor category	Variables used	Trait products
climate	mean annual temperature	BL, BG, SL, VC
	Mean temperature of warmest quarter	MM, MD
	Max. temperature of warmest month	MD
	Min. temperature of coldest month	BM, MD, VC
	Min. temperature	
	Mean temperature of the wettest quarter	VC
	Mean temperature of the driest quarter	VC
	Number of frost day per year	BG
	Temperature seasonality	SL, VC
	Temperature annual range	SL
	Mean diurnal temperature range	VC
	Annual temperature range	VC
	Mean diurnal/ mean annual temp. range (isothermality)	MM, VC
	Annual net radiation	BG
	annual total solar radiation	BL
	Daily mean solar radiation	VC
	Mean annual precipitation	MD, BG, SL, VC
	precipitation/evapotranspiration (aridity index)	BL, BM, BG, VC
	precipitation seasonality	BM, MM, SL
	precipitation in the driest quarter	BM, MM, VC
	precipitation in the driest month	MM, VC
	precipitation in the wettest quarter	MM
	Precipitation of the driest month	VC
	Precipitation of the warmest quarter	VC
	Precipitation of the coldest quarter	VC
	Min. June-july-august precipitation	VC
	Max. June-july-august precipitation	VC
	Precipitation annual range	SL
	Evapotranspiration seasonality	VC
	Mean annual evapotranspiration	VC
	Evaporative demand	BG
soil	pH (H2O)	BL, BM, BG, VC
	pH (CaCl2)	VC
	pH (KCl)	VC
	clay content	BL
	CEC (soil cation exchange capacity)	BM, BG, VC
	Soil texture	BG
	Total N	BG
	C/N	BG
	Net N mineralization rate	BG
	Base saturation	VC
	CaCo3	VC
	Exchangeable Al, Ca, H, K	VC
	Total K	VC
atmosphere	Dry, wet, total inorganic N deposition	VC
	dry oxidate N deposition	VC
topography	Elevation	MM, VC
satellite surface reflectance	EVImax, EVIstd, NDWImax, median of MODIS reflectance bands 2, 5, 6	MM
In-situ image observations	RGB images (iNaturalist)	SL

Table S2: Overview of products used for predicting global trait patterns. GSDE was developed by Shangguan et al. (2014). The abbreviations of trait upscaling products is as in Table S1.

Predictor category	Product name	Trait products using it
Climate	CRU	BL, BG
	WorldClim	MM, VC, SL, MD
	CHELSA	BM
soil	SoilGrids	BM
	IGBP-DIS	BG
	ISRIC-WISE	BL
	GSDE	VC
Land cover	MODIS	MM, MD
	ESA-CCI	VC
	CLM (Oleson et al. (2013), MODIS-based)	BL

Table S3: Overview of sources of global upscaled foliar trait maps.

Lead author	access
Bodegom	Personal communication
Butler	https://github.com/abhirupdatta/global_maps_of_plant_traits
Madani	http://files.ntsg.umt.edu/data/Global_Key_Traits/
Moreno	https://www.try-db.org/TryWeb/Data.php#59 https://www.try-db.org/TryWeb/Data.php#60
Boonman	http://doi.org/10.6084/m9.figshare.11559852
Vallicrosa	https://doi.org/10.5281/zenodo.7825970
Schiller	https://doi.org/10.6084/m9.figshare.13312040.v1

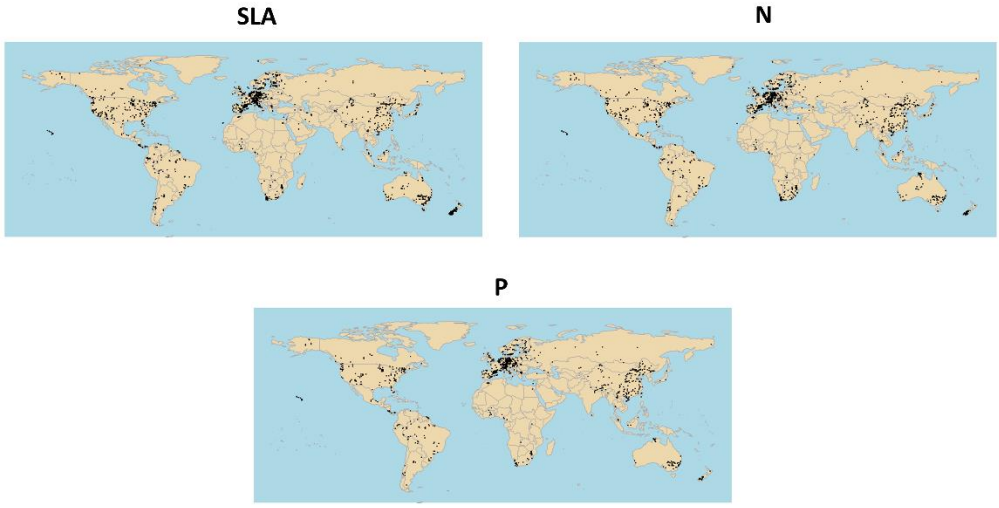

Figure S1: Location of reference grid cells. *The data from all upscaling approaches were combined here for the sake of simple illustration.*

Text S1: Overview of upscaling methods

The seven products represent a broad range of motivations, from supporting land surface modeling (Butler, Madani and Moreno), or predicting future changes in foliar traits under climate change (Madani, Boonman and Vallicrosa), to characterizing functional biodiversity (Boonman, Schiller). The Bodegom map was developed to test the potential of estimating vegetation-type distribution from foliar trait maps. The purpose of the Schiller maps was to demonstrate the potential of using citizen science observations for global trait mapping. All seven studies had in common that they were 'data-driven', i.e., statistically upscaled from in-situ observations, in contrast to more process-based approaches used in some global vegetation models (Goll et al., 2017; Thum et al., 2019; Zaehle and Friend, 2010).

From leaf to grid cell

This step transforms the in-situ leaf-level trait values to the canopy level and then the grid scale, with the resulting grid-level estimate intended to be a value representative of the entire grid cell that can be used for training the regression model in the spatialization step. The approaches differ both in the selection and pre-processing of in-situ data, and in the way values were estimated for the grid cell.

Selection of in-situ data sources. With one exception (Bodegom), all upscaling methods relied on in-situ, leaf-level trait data from one or several large trait databases, which were partly supplemented by literature sources and forest inventory data (Fig. 1). No two methods used exactly the same in-situ dataset due to differences in the versions of the same trait database.

Pre-processing of in-situ data. All upscaling approaches applied data filtering, e.g. exclusion of observations lacking reliable geo-location information. However, outlier filtering differed significantly among approaches, and some studies used elaborate data selection strategies (Boonman) and others applied gap-filling techniques (Moreno).

Estimation of grid-cell-level trait values from in-situ observations. In general, the motivation for each product guided the approach used to appropriately represent trait values for vegetation canopies at the resolution of the grid cells. Approaches motivated by land surface modeling accounted for within grid trait variations by using plant functional type (PFT) information to split data into PFTs and/or calculate cover-weighted averages (Butler, Madani, Moreno, Vallicrosa). The term 'PFT information' is used to include both the in-situ PFT categories obtained from the trait databases and the remote sensing-derived, top-of-canopy PFT cover maps (Table S2). Approaches with a focus on characterizing biodiversity either calculated plant community averages of traits and then further averaged the community averages within each grid cell (Boonman), or combined all available in-situ trait data for the reference grid cells without any weighting (Bodegom). No abundance or other weighting was applied in the averaging operations in the upscaling approaches without PFT information.

Grid-cell size: The spatial resolution differed considerably. Four maps were provided at 0.5° (~50 km at the equator), one at 0.05° (~5 km at the equator) and two maps at the resolution of 1 km (Table 1).

Number of resulting reference grid cells. There is a considerable range in the number of reference grid cells due to differences in the in-situ data. While the earliest global upscaled maps (Bodegom) used about 200 reference grid cells, the more recent ones (Moreno, Vallicrosa) used about 800 and 1400 reference grid cells respectively. The

geographical distribution of reference grid cells is strongly biased towards Europe and to a lesser degree North America and East Asia (Fig. S1).

Spatialization: from spatially sparse data to the global vegetated land surface

This step involves predictive mapping using a regression-based approach in which models are either trained on the reference grid cells or, in the case of Schiller, the leaf-level trait data to establish relationships between the traits and predictor variables.

Selection of predictor variables. Common predictors among all approaches are climate data, with additional variables including land cover types, soil characteristics (type, structural and chemical properties) and remote sensing data such as multispectral reflectance or spectral vegetation indices (Fig. 1). The most commonly used predictors were related to temperature, precipitation, solar radiation, soil pH and cation exchange capacity (Table S1). The sources for climate, soil, and land cover differed among studies (Table S2). All maps used environmental predictors in the spatialization

Statistical algorithms used in the mapping step. The algorithms used for regression-based mapping included standard multiple regression, generalized additive and linear models, as well as machine learning algorithms such as random forests and neural networks. While most studies relied on a single algorithm for the final trait maps, one study used an ensemble approach that included four different algorithms (Boonman). Butler was the only approach that explicitly took spatial information into account (Datta et al., 2016), which effectively amounted to a regression-kriging approach (Hengl et al., 2007).

Global coverage. The degree of completeness of the spatial coverage of the maps differed. Four maps provided gap-free global maps (Bodegom, Butler, Madani, Boonman), while the two high-resolution maps excluded cropland (Moreno, Vallicrosa). Schiller had gaps in different regions due to the availability/selection of plant photographs from iNaturalist. All upscaling approaches except Madani only considered trait variation in natural vegetation and excluded foliar traits in croplands. While most approaches considered vegetation of different growth forms, Vallicrosa only mapped traits for woody vegetation (Table 1).

Part 2

Additional information on **methods used in this study**

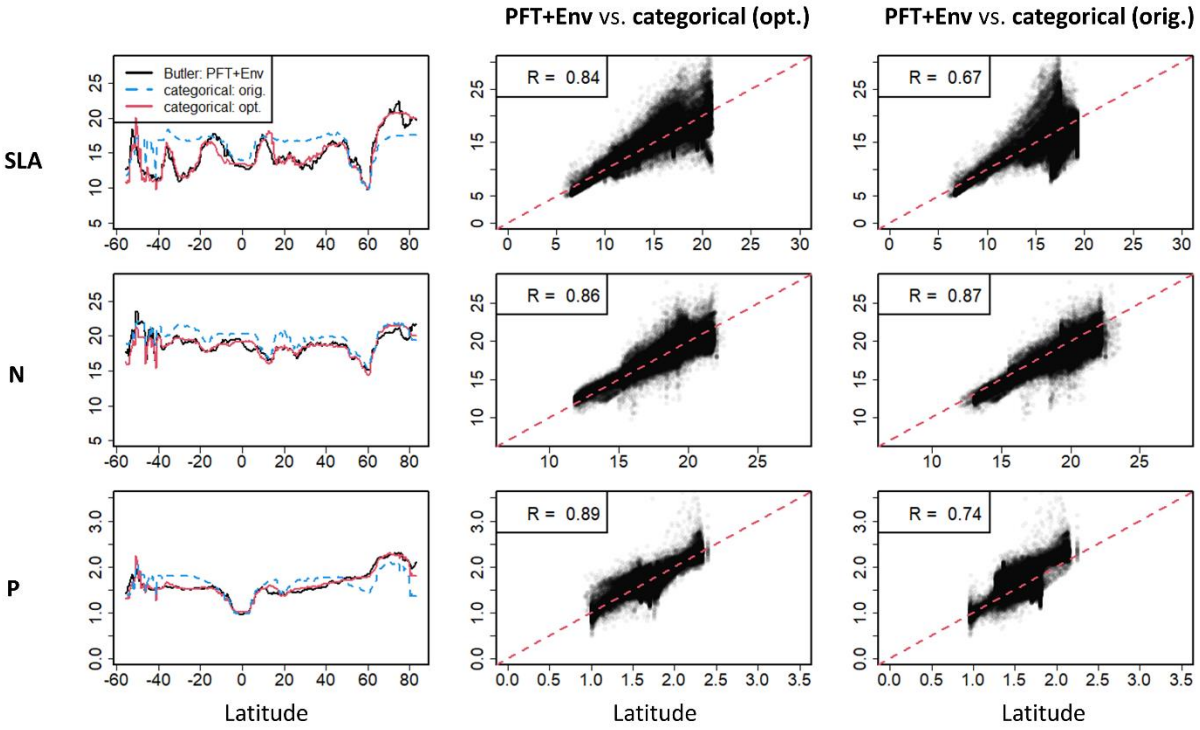

Figure S2: Comparison of the upscaled PFT+Env Butler maps with the categorical map (´PFT´ in Fig. 7a) generated by Butler (´orig.´) using TRY data and the optimized (´opt.´) categorical map with values adjusted to better match the full upscaled PFT+Env map.

Text S2: Details for methods to quantify trait variations within PFTs.

Trait heterogeneity filtering. For this approach, we combined the PFT-mean trait values with global maps of land cover fractions for each grid cell, both provided by Butler and originally based on the TRY database (Kattge et al., 2020, 2011) and MODIS and AVHRR satellite products of land cover (Lawrence and Chase, 2007). For each 0.5° grid cell, we then estimated the trait variability by calculating the coefficient of variation (CV) of a variable in which each PFT mean trait value was represented proportional to its land cover fraction (Fig. S3). For each trait, we categorized grid cells with higher CV than the median of all grid cells as 'heterogeneous' and those with lower CV than the median as 'homogeneous'.

Unmixing. This approach entails essentially reverse engineering the final step of calculating grid-cell averages weighted by land cover in the generation of some of the 'PFT+Env' trait maps (Fig. 1). While not all maps applied the LCT weighting after the spatialization, this approach can be applied to all maps as the only assumption is the linear mixing of LCTs, i.e. only the spatial distribution of land cover is used. The unmixing was done by using a three by three grid cell moving window within which the system of overdetermined linear equations for six PFTs (ENF, DNF, EBF, DBF, SHR, GRA) was solved. For each grid-cell, there is one linear equation that equates the final grid cell trait value (known) with the sum over the six products of fractional land cover (known) times the corresponding local, PFT-specific trait value (unknown). For solving the linear equation systems the function *lsei* of the R package *limSolve* was used in combination with the *focal* function of the *terra* package (Hijmans et al., 2015; Soetart et al., 2022; Van den Meersche et al., 2009). We evaluated the performance of the unmixing approach with the categorical ('PFT') maps provided by Butler and found that it performed robustly for ENF and DNF, and reasonably well for DBF and EBF but could not be used for SHR and GRA (Fig. S4a). The limitations for SHR and GRA are likely due to their broad trait distributions and their co-occurrence with other LCTs with similar

trait values. To exclude grid cells where the unmixing method did not work well, we applied a threshold on the fractional cover of the relevant PFT of 5% and applied thresholds on the maximum and minimum possible trait values to exclude large outliers or ecologically implausible values. Even after this filtering step, considerably more data were left for analyses of ENF and DBF than in case of applying the trait heterogeneity filtering approach.

Overall approach. Due to the limitations of both approaches for some LCTs, we combined the unmixing approach for ENF, DBF, and EBF with the trait heterogeneity filtering approach for SHR and GRA. For EBF, we chose unmixing as it provided better coverage.

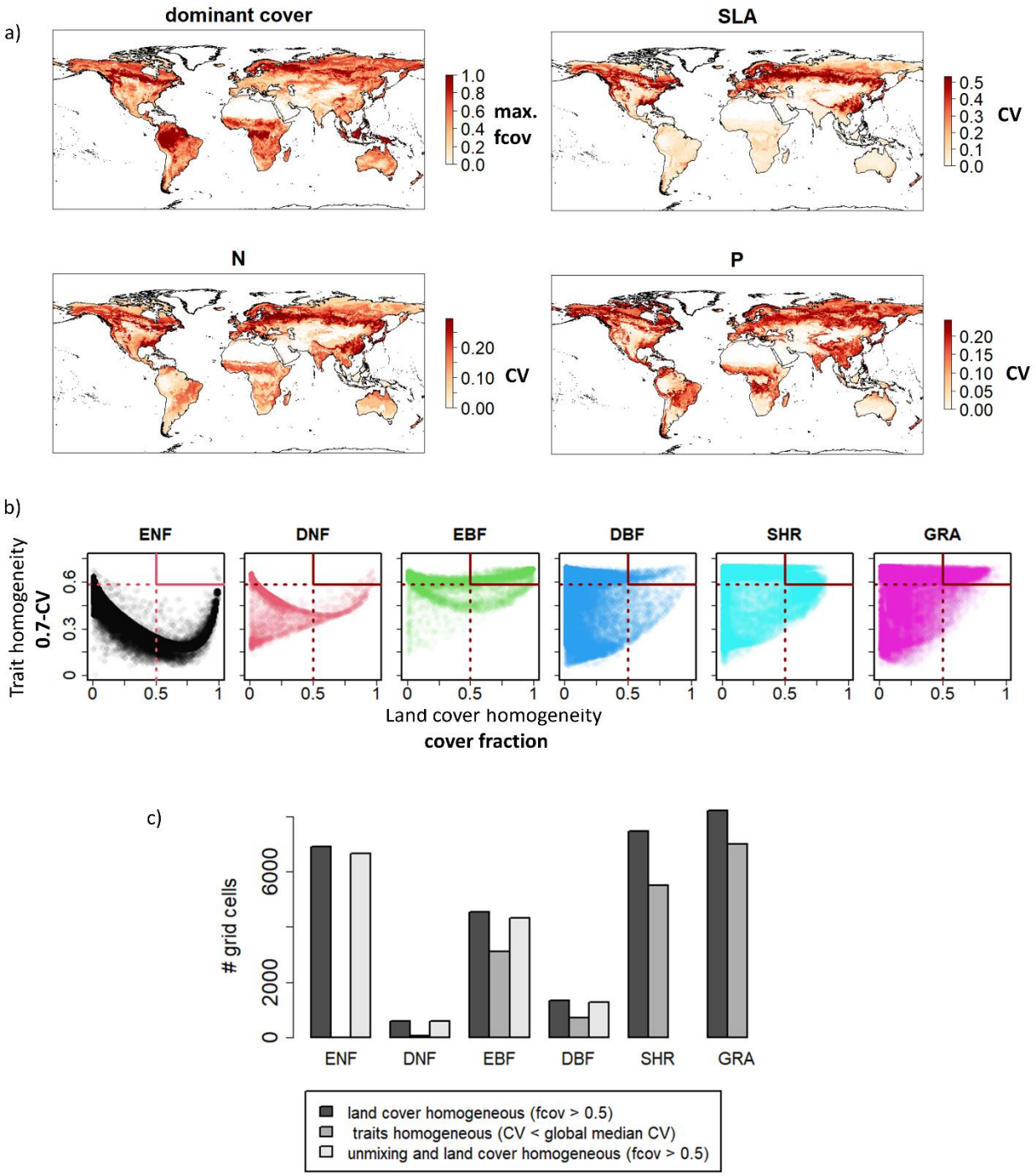

Figure S3: Overview of estimated within grid cell trait variability and its relationship with land cover homogeneity. a) estimates of within grid cell coefficient of variation maps are shown for each trait. For reference, the maximum fractional cover over all landcover types in a given grid cell (´dominant cover´) is shown. b) relationships between the within-grid-cell trait homogeneity (0.7-CV) vs. land cover homogeneity (cover fraction) per land cover type for SLA. Thresholds on both axes illustrate which data would remain (upper right hand corner with continuous red lines) after such a selection based on a minimum of 50% cover and a level of homogeneity exceeding the global median. c) overview of impact on the land cover and trait homogeneity thresholds on remaining vegetated grid cells at the global scale together with unmixing results (for SLA). Note that unmixing results can be used also at lower cover thresholds. In c) the bar for the ´traits homogeneous´ category was slightly increased to make it visible.

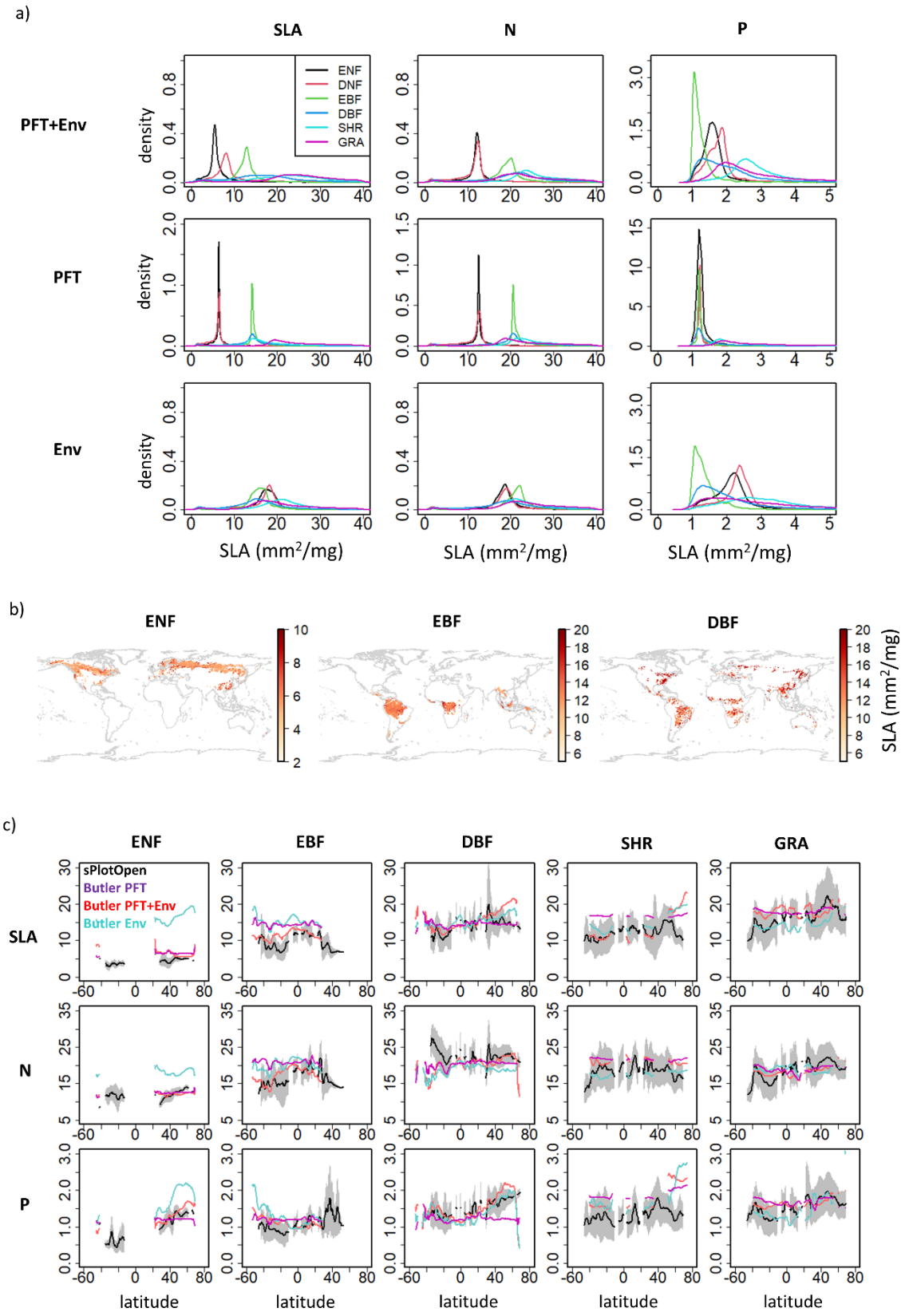

Figure S4: Unmixing results based on different versions of the Butler maps. The categorical case ('PFT') can serve as a reference as for each PFT one to three discrete values were assigned. a) trait distributions from unmixing. b) unmixed PFT maps for Butler PFT+Env for SLA. c) comparison of combined unmixing/trait heterogeneity filtering to sPlotOpen TWM reference data.

Table S4: Threshold criteria to assign dominant plant functional type (PFT) categories to sPlotOpen plots. *The approach follows the definition of forests by the FAO to apply a 10% threshold on the cumulative ('cum.') cover of trees. The PFT classification of plots was only applied if growth form information was available for at least 50% cumulative cover. PFT abbreviations are as follows: ENF: evergreen needleleaf forest; EBF: evergreen broadleaf forest; DBF: deciduous broadleaf forest; SHR: shrubland; GRA: grassland.*

PFT	**Criteria**
Forest	Cum. cover of tree species > 10 %
ENF	Forest + cum. cover of needleleaf species > 70% AND cum. cover of evergreen species >70 %
EBF	Forest + cum. cover of broadleaf species > 70% AND cum. cover of evergreen species >70 %
DBF	Foret + cum. cover of broadleaf species > 70% AND cum. cover of deciduous species >70 %
DNF	Forest + cum. cover of needleleaf species > 70% AND cum. cover of deciduous species >70 %
SHR	Cum. cover of shrub species > 10 %
GRA	Other than forest, shrubland and wetland PFTs

Part 3

additional **Results**

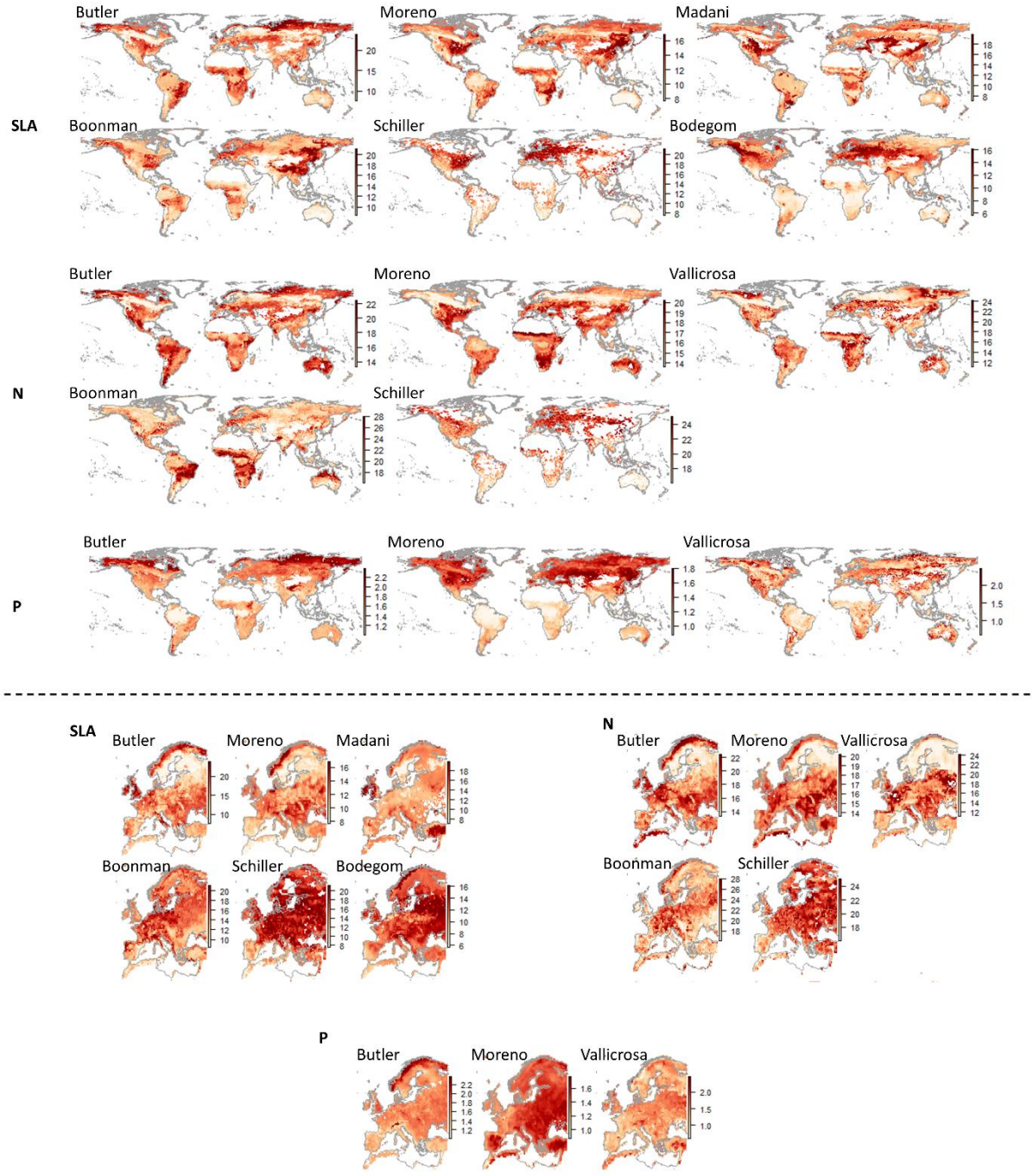

Figure S6: Overview of all individual upscaled maps for SLA, N and P. Units are as in Fig. 5. As the maps have both different mean values and levels of variability, each map is shown with a different scale in order to facilitate the comparison of spatial patterns. Global maps are shown on top of the horizontal dashed line, detail maps of Europe are shown below the line. For each trait, the top row for shows maps based on PFT+Env upscaling approaches, the bottom rows maps based on Env upscaling approaches

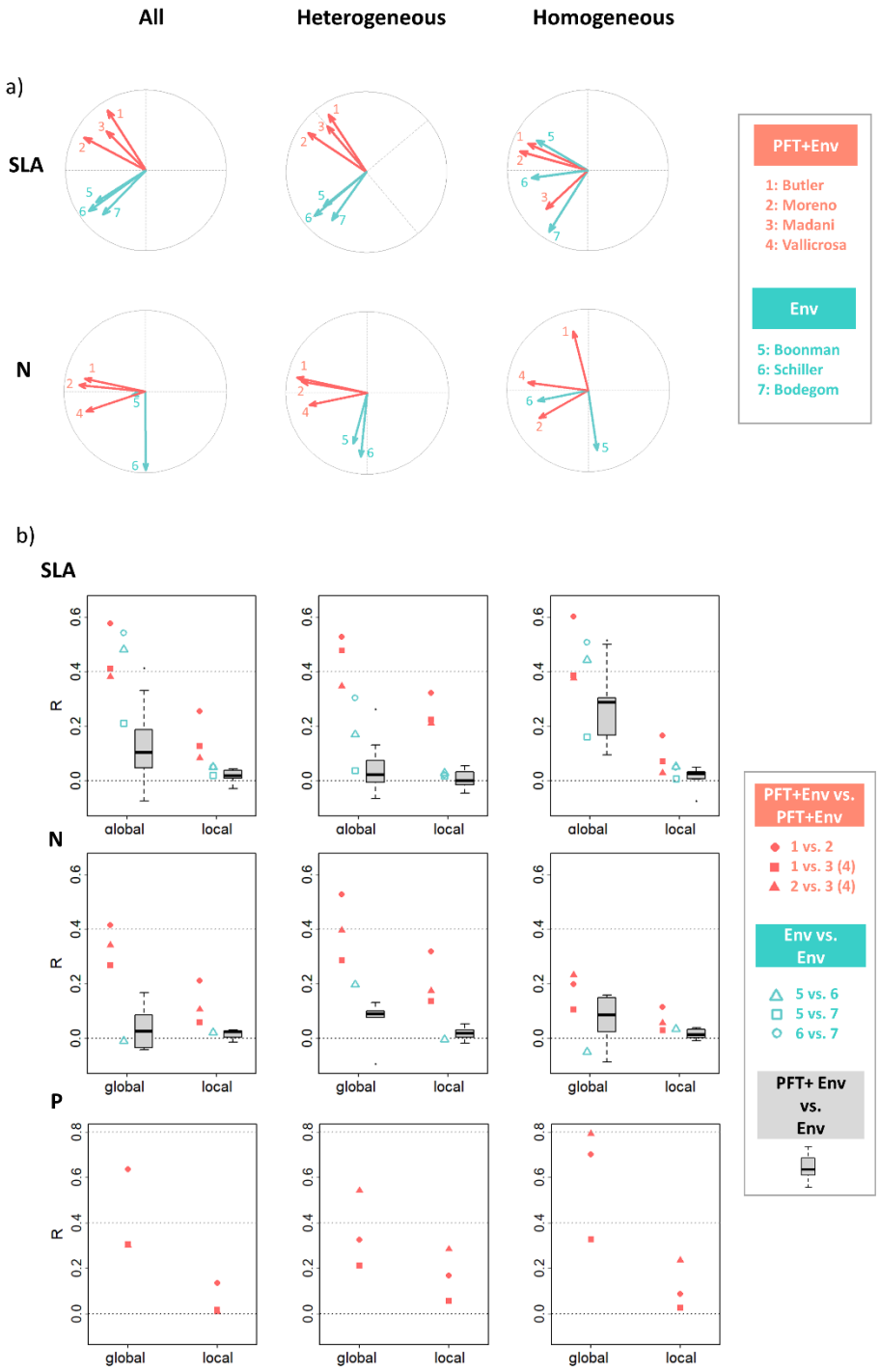

Figure S7: Overview of principal component analyses and pairwise correlation of upscaled maps for specific leaf area (SLA), leaf nitrogen (N) and phosphorus (P) concentration with different within-grid-cell heterogeneity cases. The column with all vegetated grid cells ('all') is identical to Fig. 2 *and only shown for reference here, the columns with only heterogenous or homogeneous grid cells are based on threshold on estimates of the within-grid-cell trait variability. In the principal component biplots a) and the pairwise correlation plots b), colors correspond to the use of predictor variables ('Env' stands for environmental variables, while 'PFT' stands for plant functional type and land cover type information). Pearson correlation is shown either for all selected grid cells ('global') or as median value of the local spatial correlation map in 3 x 3 pixel windows ('local'). In b) the grey boxplots contain all possible pairs of PFT+Env maps and the Env maps; for the PFT+Env maps, the same symbols are used for the cases 'x vs. 3' and 'x vs. 4', where x is either 1 or 2, since 3 is only available for SLA and 4 only for N and P; note that the symbols for P and the case '1 vs. 2' and '2 vs. 4' are so close that they are hard to distinguish visually.*

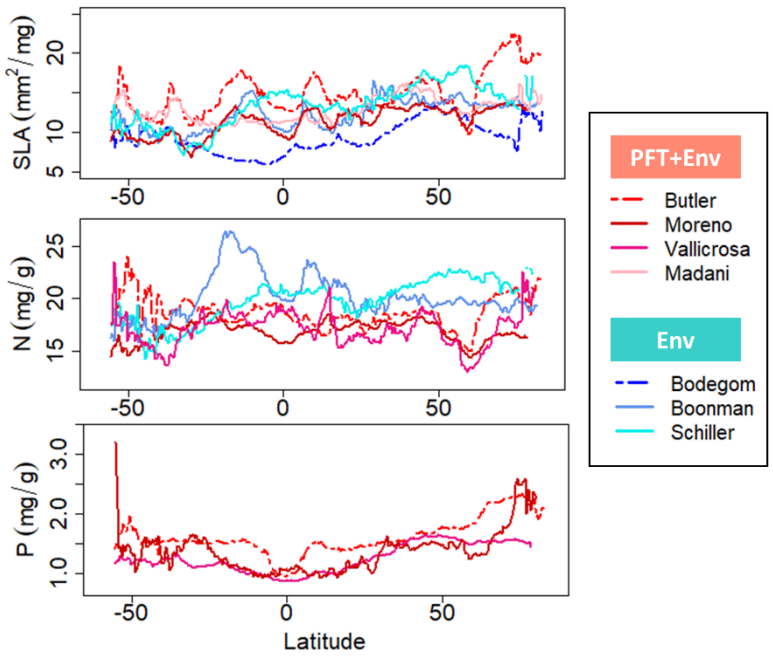

Figure S8: Overview of latitudinal median values of global upscaled trait maps. *Line colors correspond to the upscaling category (PFT+Env or Env).*

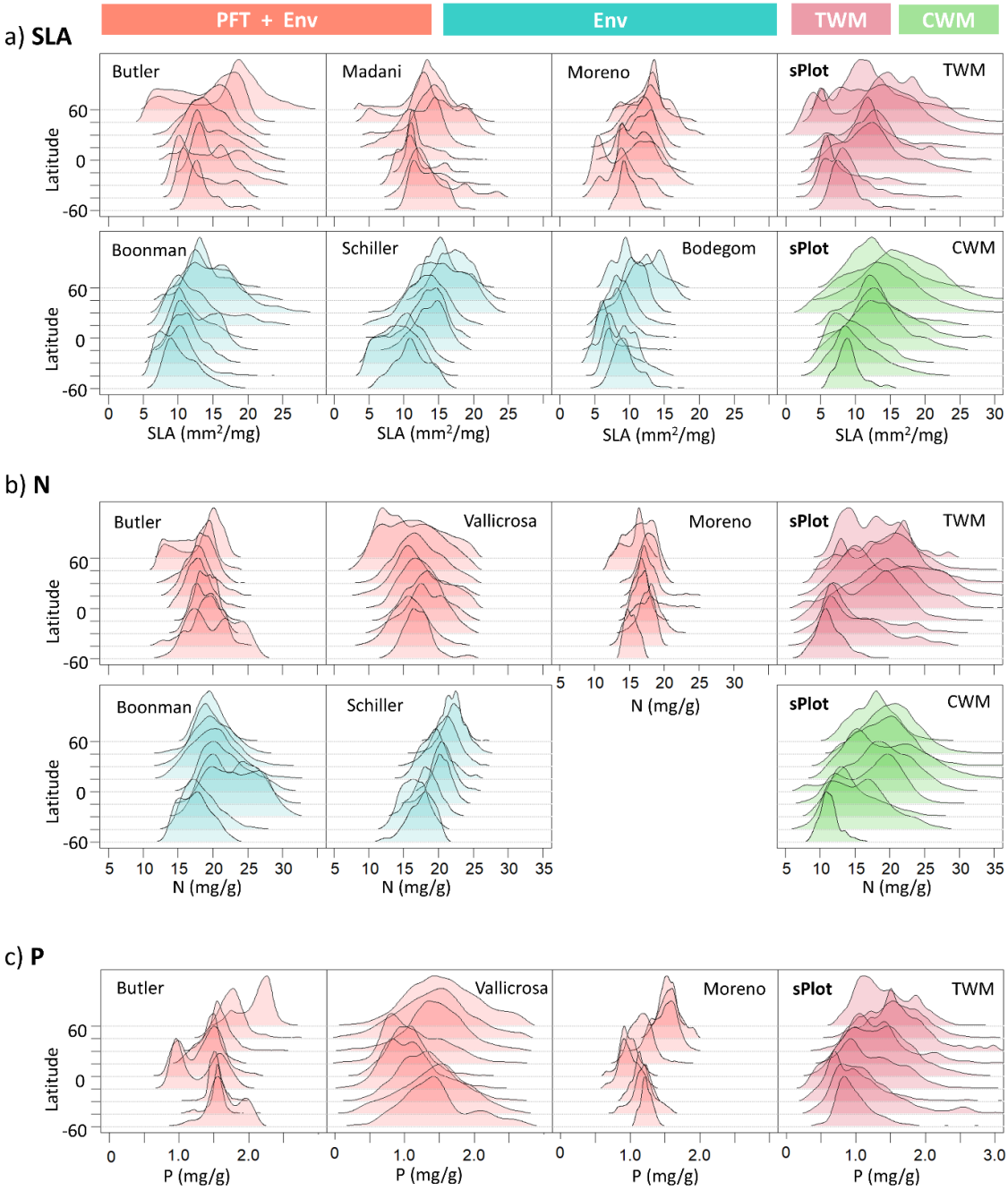

Figure S9: Latitudinal trait distributions for specific leaf area (SLA, mm²/mg), leaf nitrogen (N, mg/g) and phosphorus (P, mg/g) of upscaled maps and sPlotOpen plot-level data. *For each trait, the distributions in latitude intervals (units in degrees) are shown, with the upscaling approaches using plant functional type, land cover and environmental information (PFT+Env) in the top row in red color, and those mostly relying only on environmental information (Env) in the bottom row. Plot-level sPlotOpen ('sPlot') top-of-canopy weighted mean (TWM) are compared to the PFT+Env maps and community weighted mean (CWM) to the Env maps.*

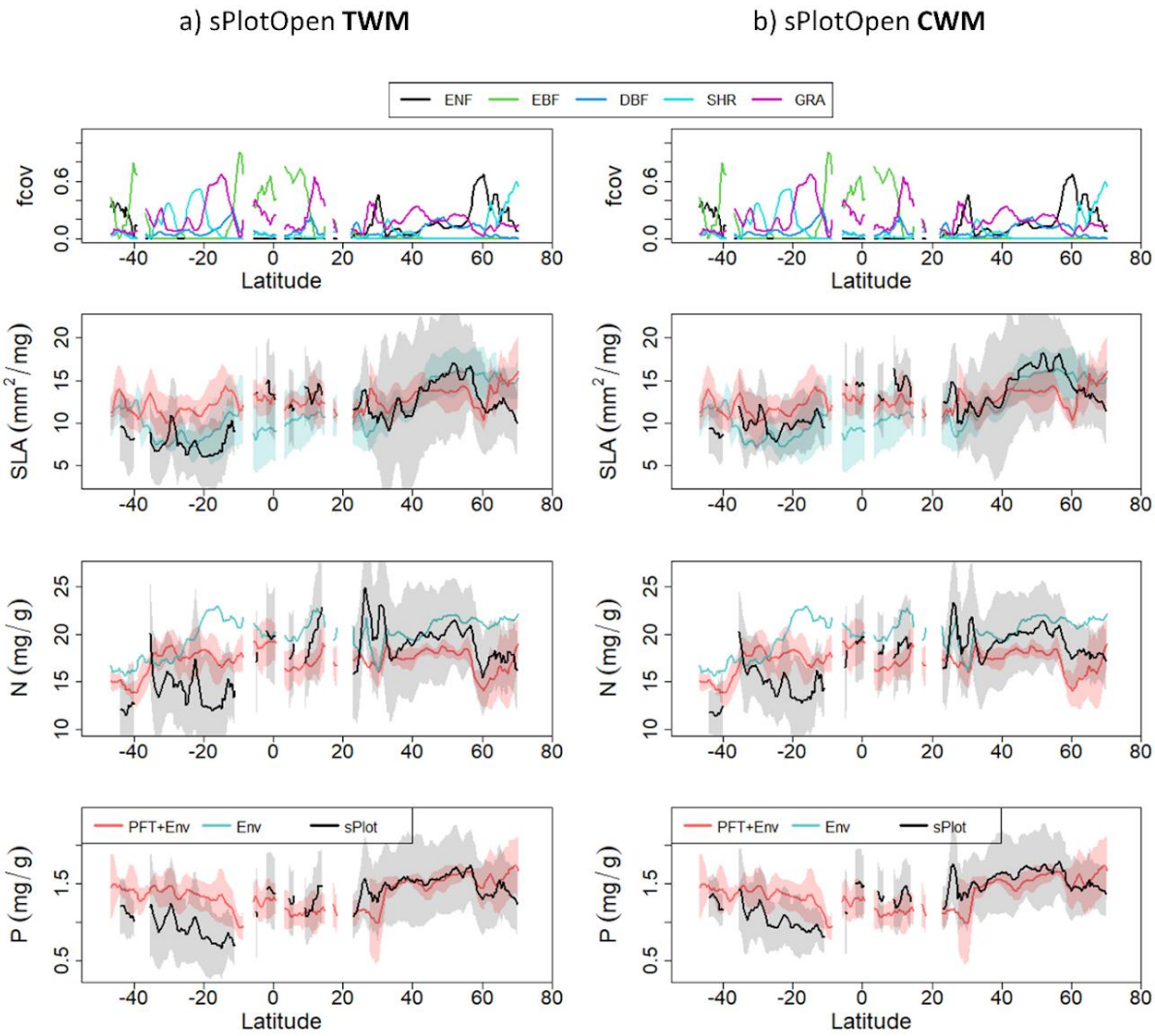

Figure S10: Comparison of latitudinal mean values of upscaled maps with plot-level sPlotOpen data. *Here, for calculating the latitudinal averages of the upscaled maps, only the grid cells in which sPlotOpen data were available were used. In the left column, sPlotOpen TWM was used to compare with PFT+Env upscaling approaches, in the right column, CWM was used to compare with Env approaches. A rolling mean was applied to all latitudinal mean values. Fractional land cover is shown on top for reference.*

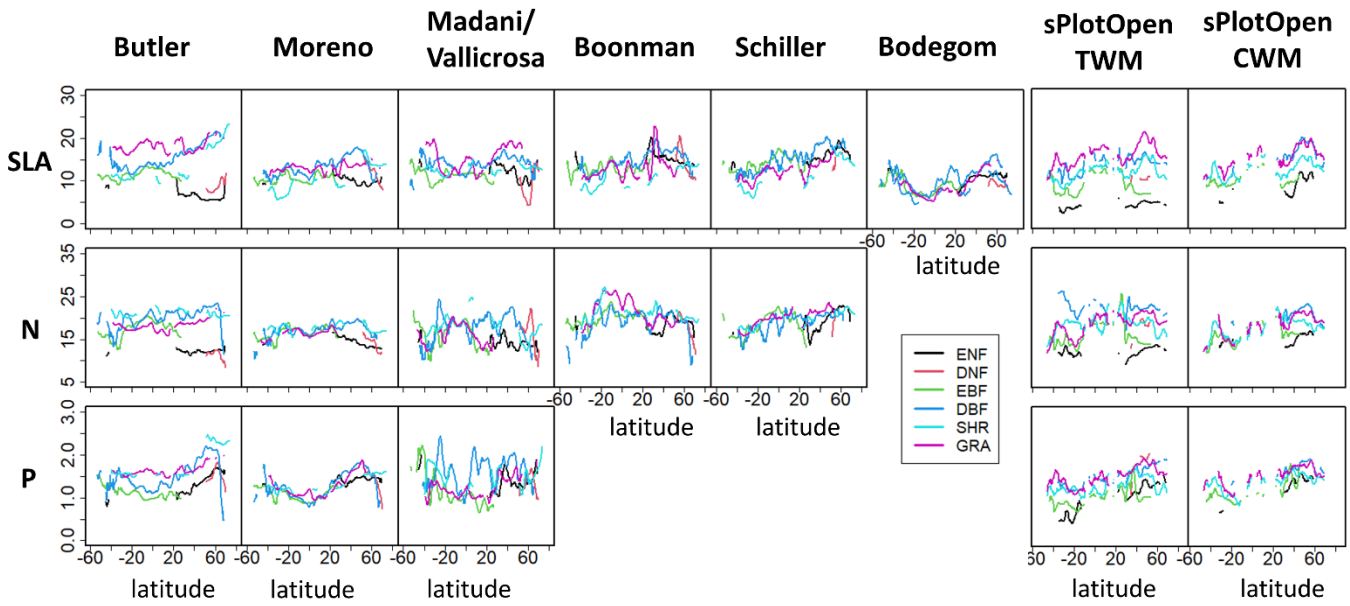

Figure S11: Overview of latitudinal trait pattern per upscaling approach with sPlotOpen data shown as reference. *The latitude range is the same for all x-axes (-50 to 80 degrees North) and y-axis scales are the same for each trait, the focus is on the relative differences between PFTs for each trait-upscaling approach combination.*

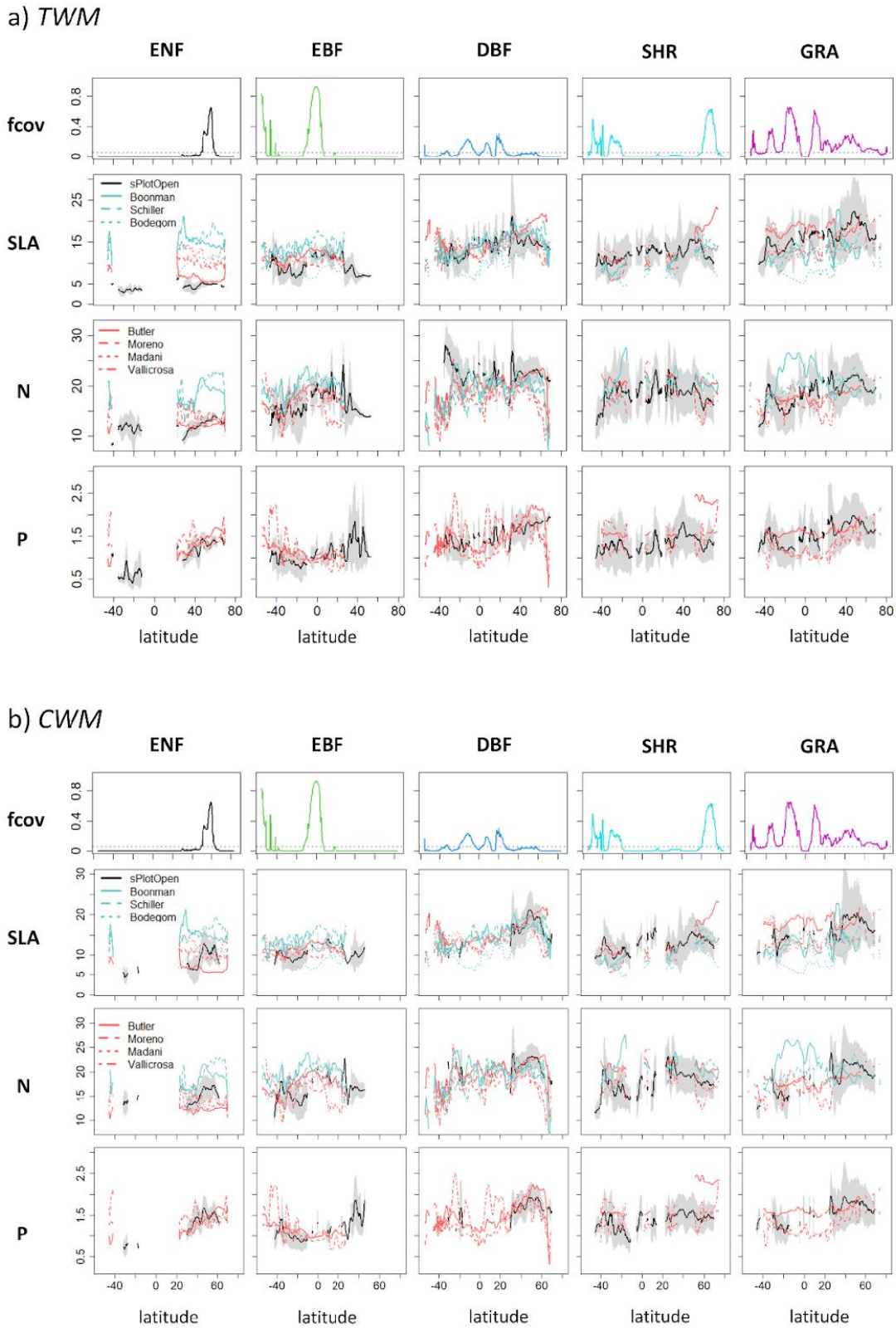

Figure S12: Comparison of latitudinal average trait patterns of upscaled maps and sPlotOpen stratified by plant functional type (PFT) and land cover type. *a) sPlotOpen top-of-canopy weighted mean (TWM) vs. upscaled maps, b) sPlotOpen community weighted mean (CWM) vs. upscaled maps. For sPlotOpen data in this analysis, the restriction of only using the PFT corresponding to the dominant PFT of the plot was not applied to maximize data coverage. The fractional land cover (fcov) is shown on top for reference with the grey dotted line indicating 5% fractional cover. The grey shaded band indicates one standard deviation from the latitudinal mean of sPlotOpen. Kernel smoothing was applied to all latitudinal averages.*

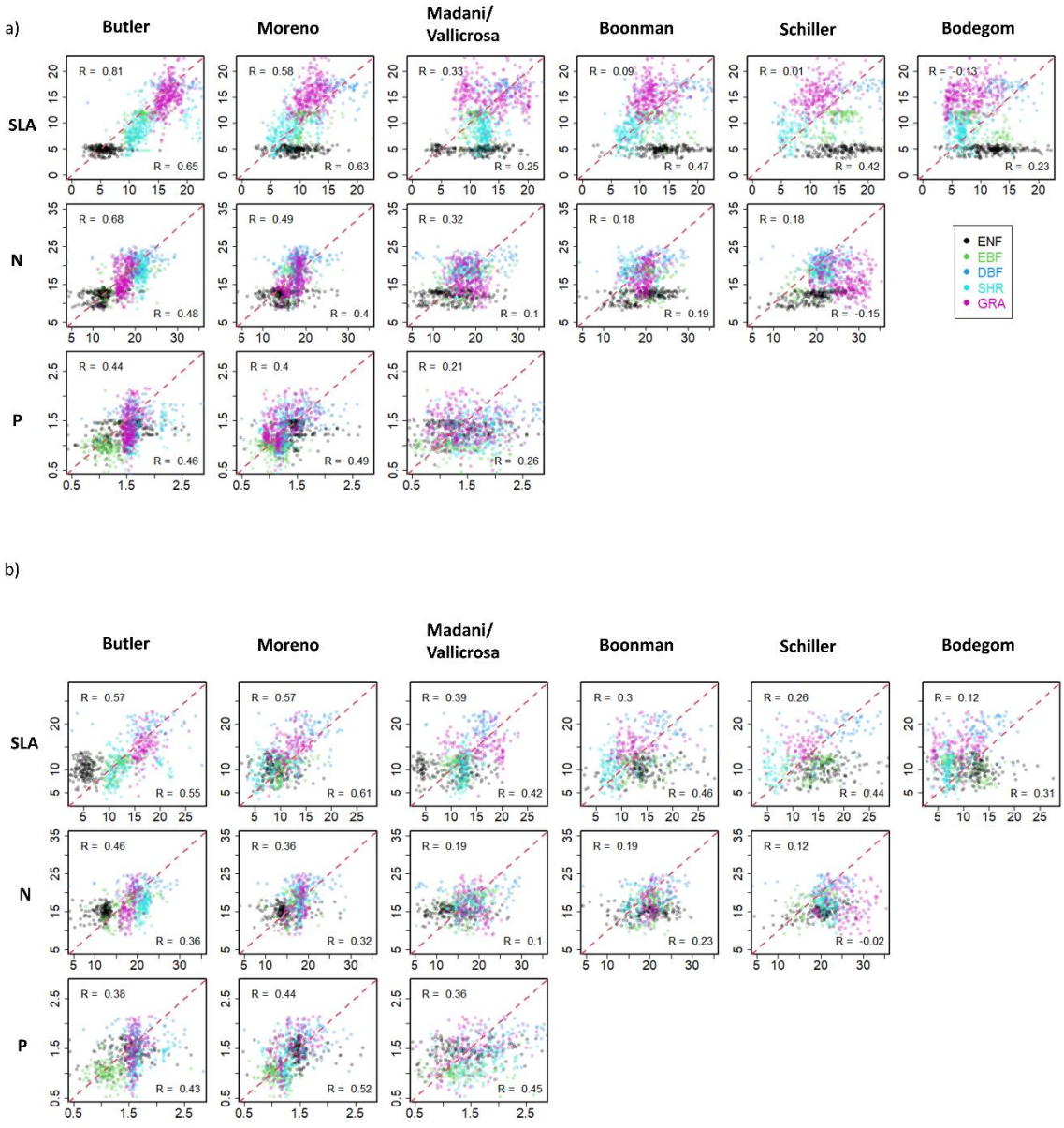

Figure S13: Comparison of upscaled maps vs. sPlotOpen stratified by PFT but with all PFTs pooled together. *For sPlotOpen either a) TWM or b) CWM was used. The correlation values in the upper left boxes indicate all PFTs pooled, the values in the lower right boxes indicates all PFTs except ENF pooled. Colors indicate the different PFTs. Units for SLA, N, and P are as in Fig. S12. A threshold of 0.5 on the land cover was applied here.*

Part 4

Additional material for the **Discussion**

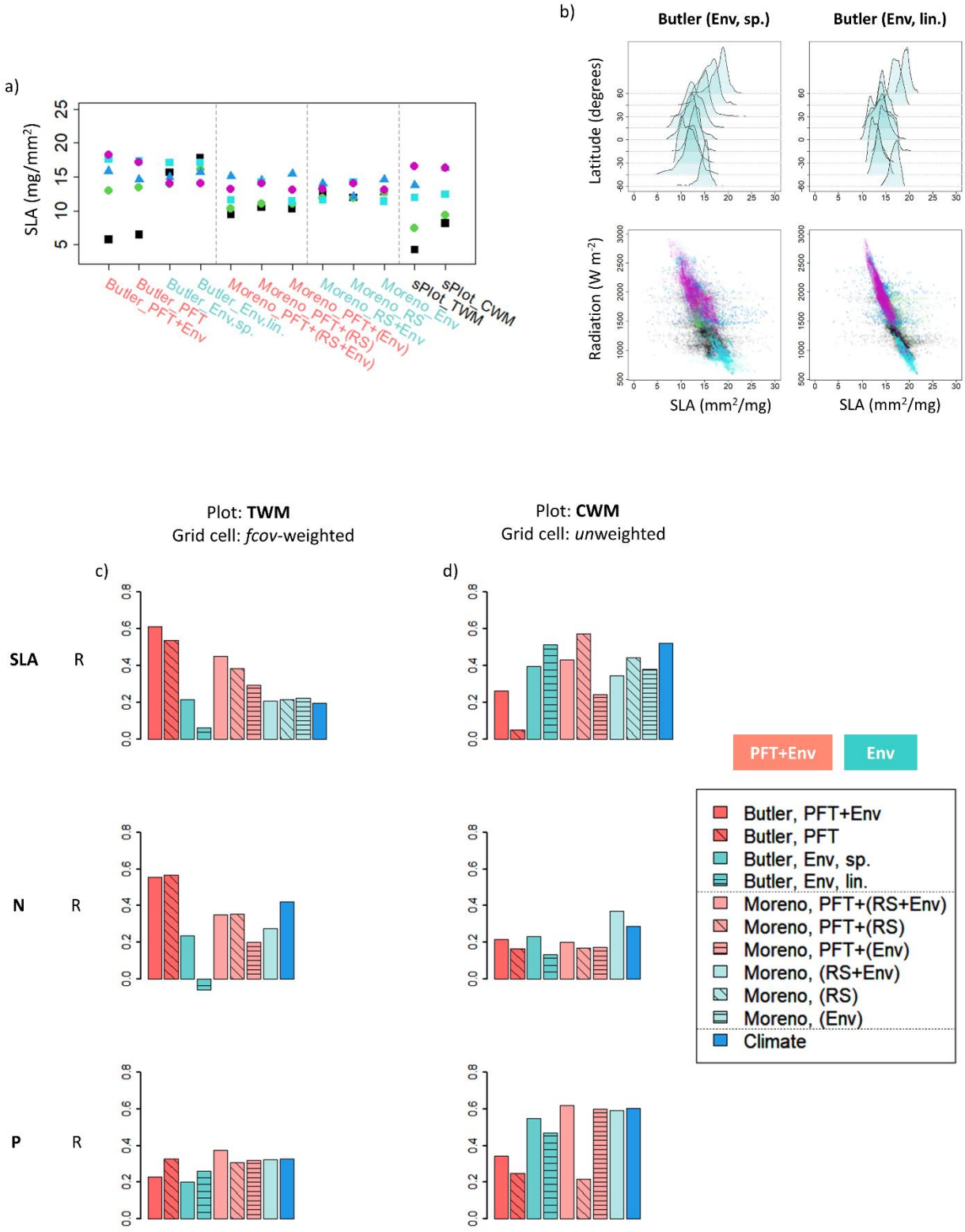

Figure S14: Overview of evaluation against sPlotOpen for different versions of Butler and Moreno using identical input data and only different upscaling approaches. *a) Overview of impact of different upscaling approaches on between-PFT trait differences for SLA; the figure corresponds to the results shown in Fig. 4b. b) Differences between using a spatial model (sp.) that corresponds to regression-kriging versus a linear model (lin.) that does not explicitly use spatial location of in-situ data in the prediction; the figure complements main Fig. 8. c) Impacts of different upscaling approaches on the agreement to sPlotOpen data scaled to the grid-cell level. The different versions of the Butler and Moreno maps correspond to those shown in Fig. S5 and the figure adds additional findings to main Fig. 6. The selected climate variables are identical to those in Fig. 6.*

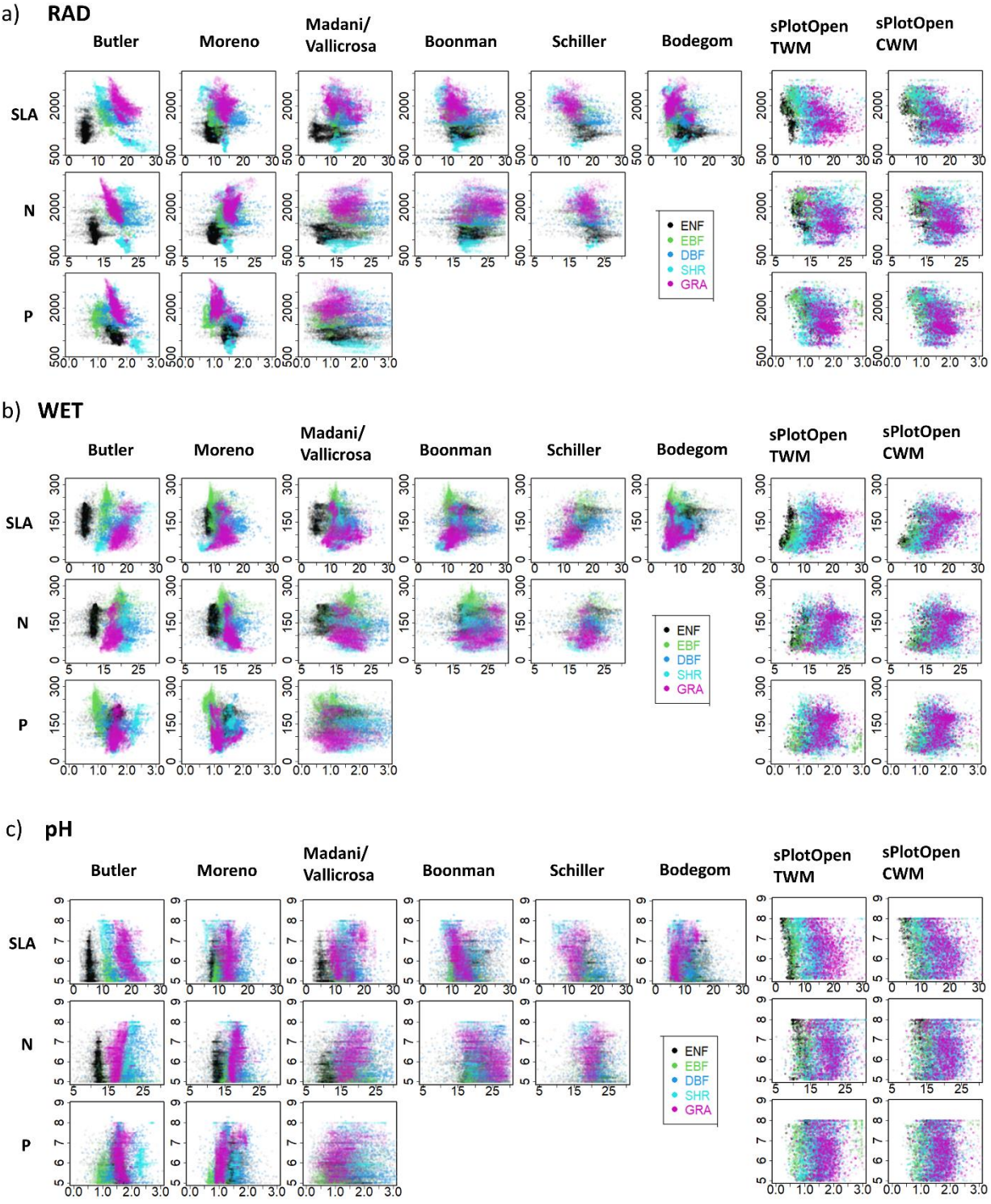

Fig. S15: Overview of trait-environment relationships for upscaled maps and sPlotOpen stratified by PFT. *a) relationships to solar radiation (RAD; units as in Fig. 6c), b) relationships to number of wet days per year (WET) according to the definition of Butler, c) relationships to soil pH. Traits are plotted on the x-axis, environmental variables on the y-axis and axes have the same range for each trait and environmental variable. Note that for sPlotOpen, plot data separately scaled to the grid cell are shown, i.e. no PFT unmixing was involved and that for the upscaled maps where the heterogeneity filtering/unmixing was applied thresholds on land cover heterogeneity and within grid cell trait variability had to be applied which likely tends to results in more separation between PFTs than is actually the case.*

Table S5: Overview of the ability of different upscaling approaches to capture between-PFT (bPFT) and within-PFT (wPFT) trait variations. *The rows show differences between mostly homogeneous (hom.) as a hypothetical case or mostly heterogeneous (het.) training grid cells as a realistic case based on the actual upscaling approaches (Fig. 9a). The trait variations can be either captured either in a relative (r.) sense related to correlation or absolute (a.) sense related to RMSE. 'Potential' indicates whether vegetation traits are modeled that could occur based on environmental conditions, while 'actual' indicates that the realized vegetation traits based on the vegetation actually growing in a given location is modeled. This terminology is similar to the one used in Bonannella et al. (2022).*

	Boonman Bodegom (Schiller)	Butler cat	Butler Madani Vallicrosa	Moreno Env	Moreno
	(Env)	**(PFT+LCT) (categorical)**	**PFT+(Env, LCT)**	**(PFT, LCT)+Env**	**(PFT,LCT) +(Env+RS)**
Mostly het.	*Potential* - wPFT	**Actual** bPFT r.+a. -	**Actual** bPFT r.+a. wPFT	*Potential* bPFT r. wPFT	**Actual** bPFT r. wPFT
Mostly hom.	*Potential* bPFT r.+a. wPFT	**Actual** bPFT r.+a. -	**Actual** bPFT r.+a. wPFT	*Potential* bPFT r.+a. wPFT	**Actual** bPFT r.+a. wPFT

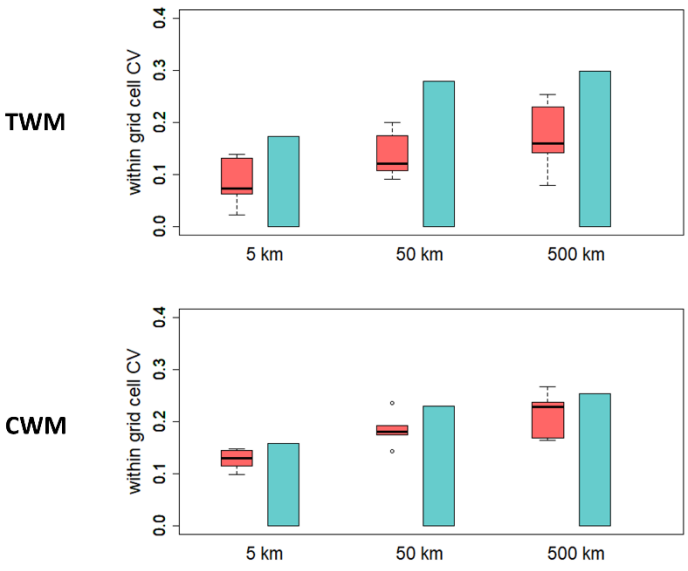

Figure S16: Overview of map uncertainty estimates provided by the upscaling approaches for SLA*. CV stands for coefficient of variation, SE stands for standard error. Note that the ways to calculate/estimate CV and SE differed considerably among maps.*

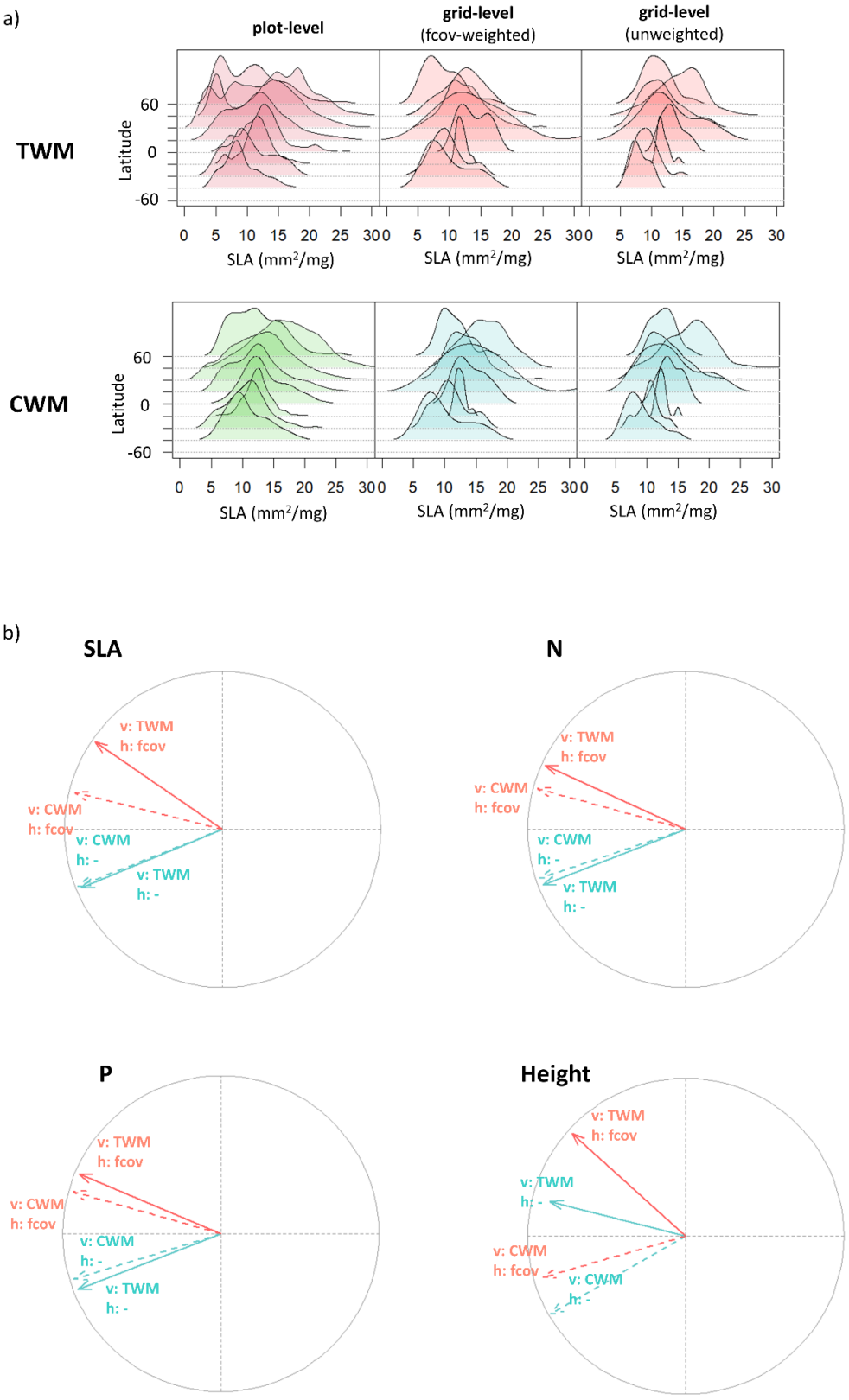

Fig. S17: Impacts of combined vertical and horizontal scaling in sPlotOpen data*. a) impact of horizontal and vertical weighting on latitudinal trait distributions of SLA for 0.5° grid cells. The trait distributions shown here differ from those in Figs. 9b and SX as a stricter data selection criterion was applied for all cases to ensure direct comparability with the fractional cover (fcov) weighting. b) PCA biplots for SLA, N, P and, for the sake of illustrating a case with extreme impact of vertical weighting, canopy height. For the vertical scaling (v:) there are two cases: CWM_all vs. CWM_toc, and for the horizontal scaling (h:) too: fcov weighting vs. no weighting indicated by "-".*

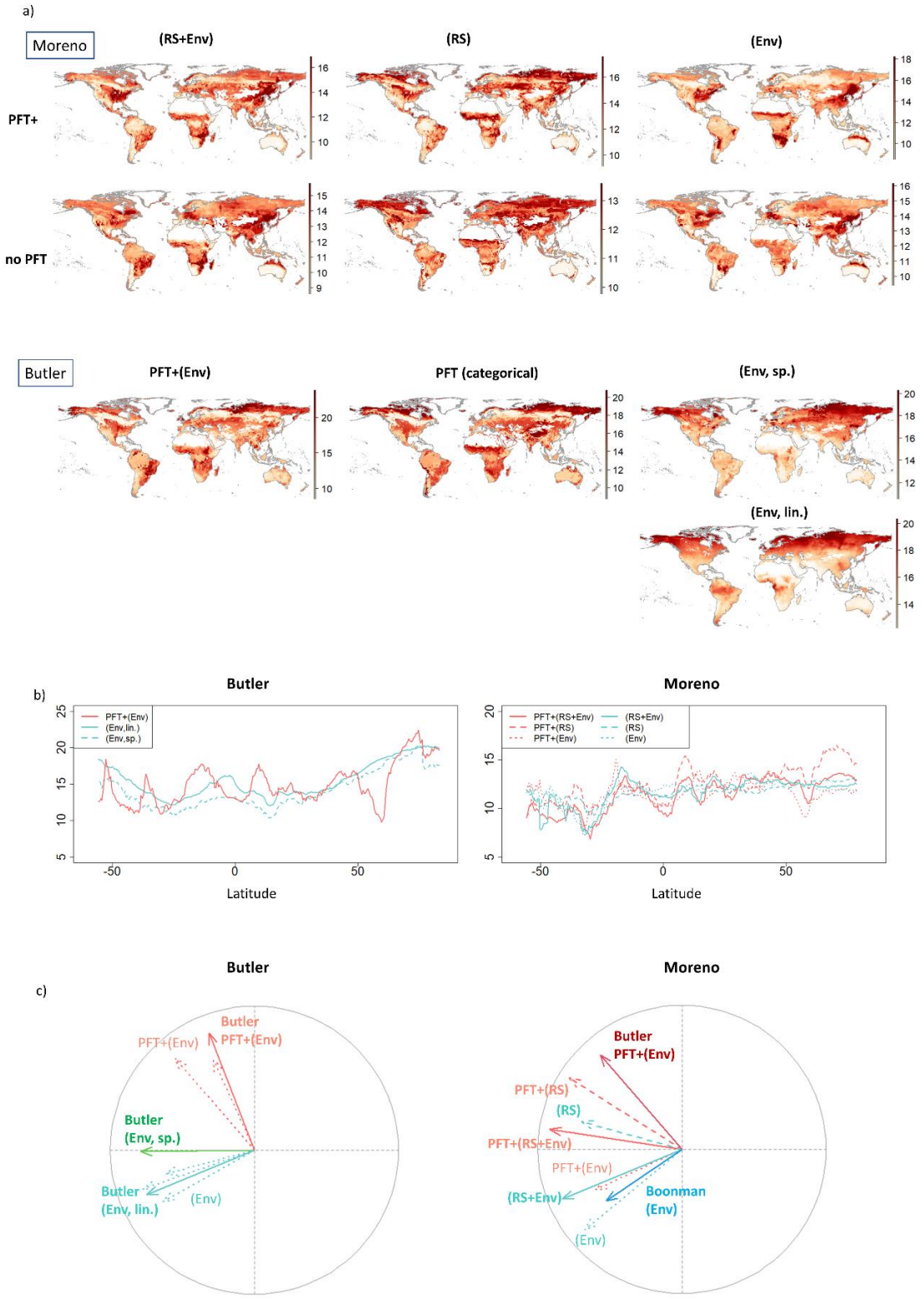

Figure S18: Overview of different versions of the Butler and Moreno maps for SLA. *a) global maps, the categorical map is the one with optimized trait values. For Moreno, the top row always includes PFT in the leaf-to-grid scaling, while PFT is not used in the second row. The symbolic notation is PFT + (X) where X represents the predictors in the spatialization. For Moreno, remote sensing (RS) predictors are based on satellite land surface reflectance observations. b) latitudinal median values, c) PCA biplots similar to Fig. 3a, other maps are added for reference to see in which groups the different versions of Butler and Moreno are falling; in the biplot for Butler, dotted arrows are used for other maps shown for reference, in the biplot for Moreno the different versions Moreno maps are shown as continuous, dashed and dotted arrows, while the reference maps are shown as continuous arrows but with other colors. For Butler linear (lin.) and spatial (sp.) Env maps are shown.*

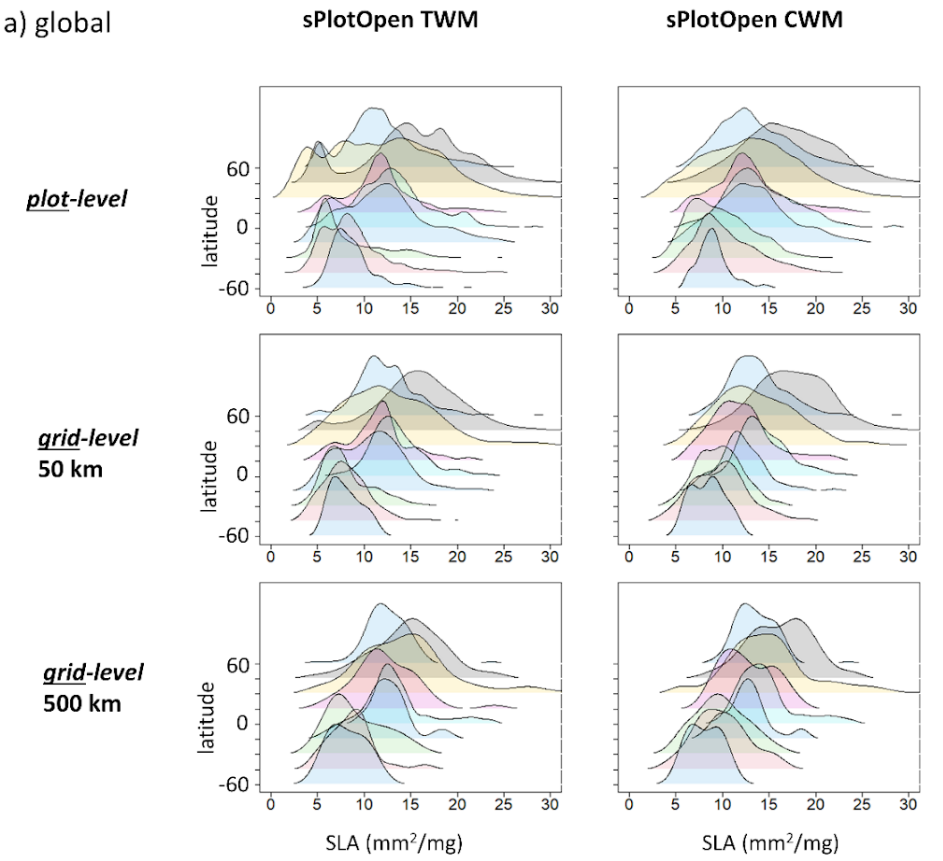

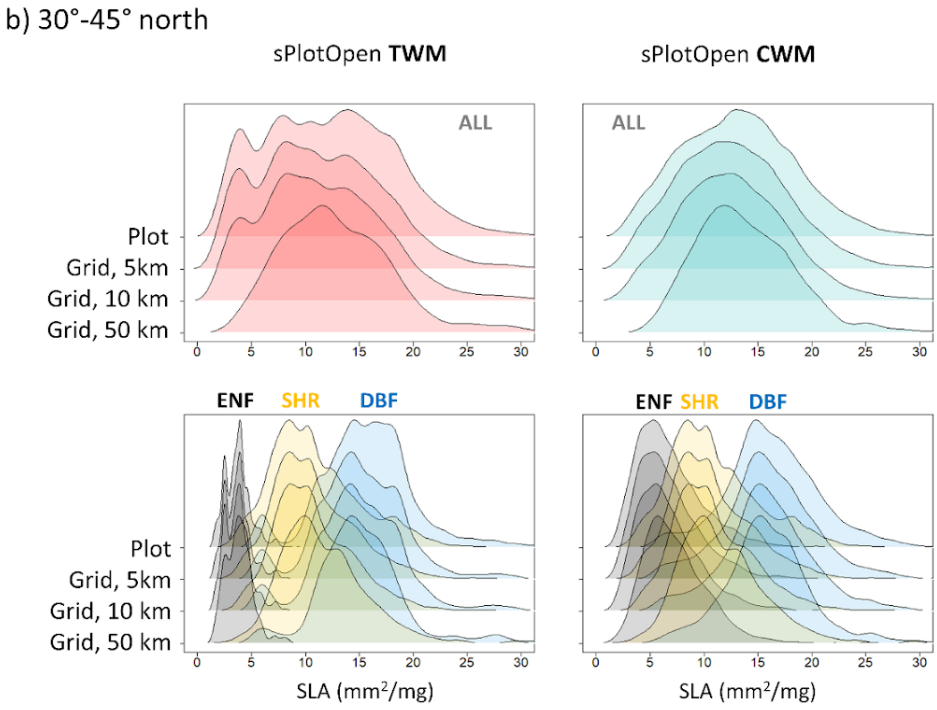

Figure S19: Dependence of latitudinal trait distributions of sPlotOpen on the grid cell size for specific leaf area (SLA). *All trait distributions are maximum-normalized. a) global-scale sPlotOpen data, b) 30-45 degree latitude interval. Note that the grid cell sizes in b) differ from those of Fig. 8b and show substantial impacts on the TWM distributions already at 50 km grid size.*

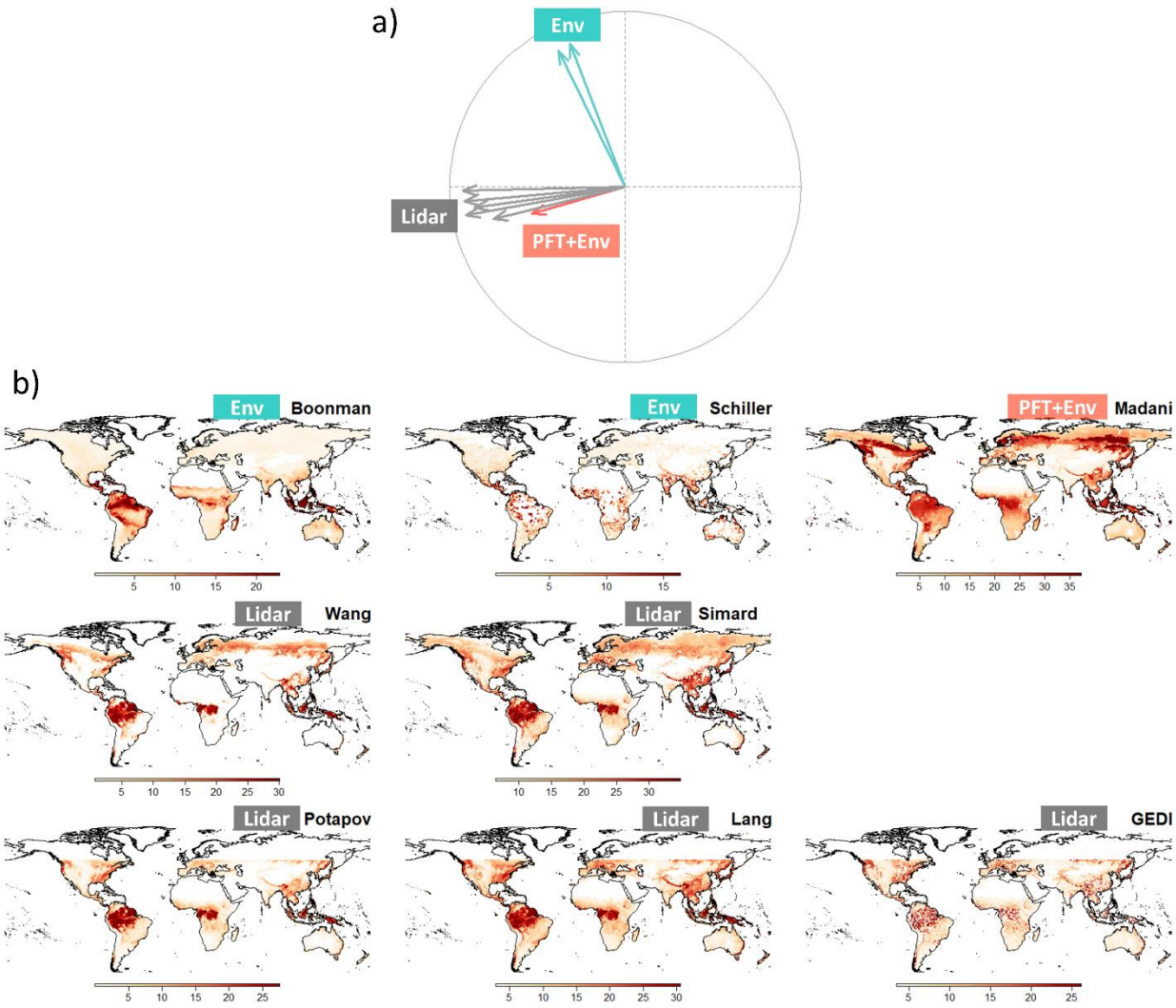

Figure S20: Overview of canopy height map based on different upscaling approaches (PFT+Env or Env) and satellite remote sensing (Lidar). *a) PCA biplot with the first two axes (explaining 72% of the variability). b) height mapswith units of meters. The lidar products refer to canopy top height maps from the publications of Wang et al. (2016), Simard et al. (2011), Potapov et al. (2021), Lang et al. (2021), and the official GEDI product (NASA). The middle row is based on data from the GLAS sensor on ICESat, while the bottom row is based on data from the GEDI instrument onboard the ISS.*

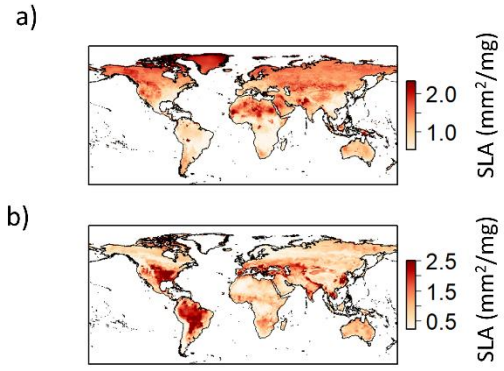

Figure S21: Example of uncertainty estimates provided by a) the Bodegom and b) the Madani upscaling approaches for SLA. *Standard error is shown. Note that Bodegom only used environmental predictors (Env) while Madani additionally used PFT information (Env+PFT).*

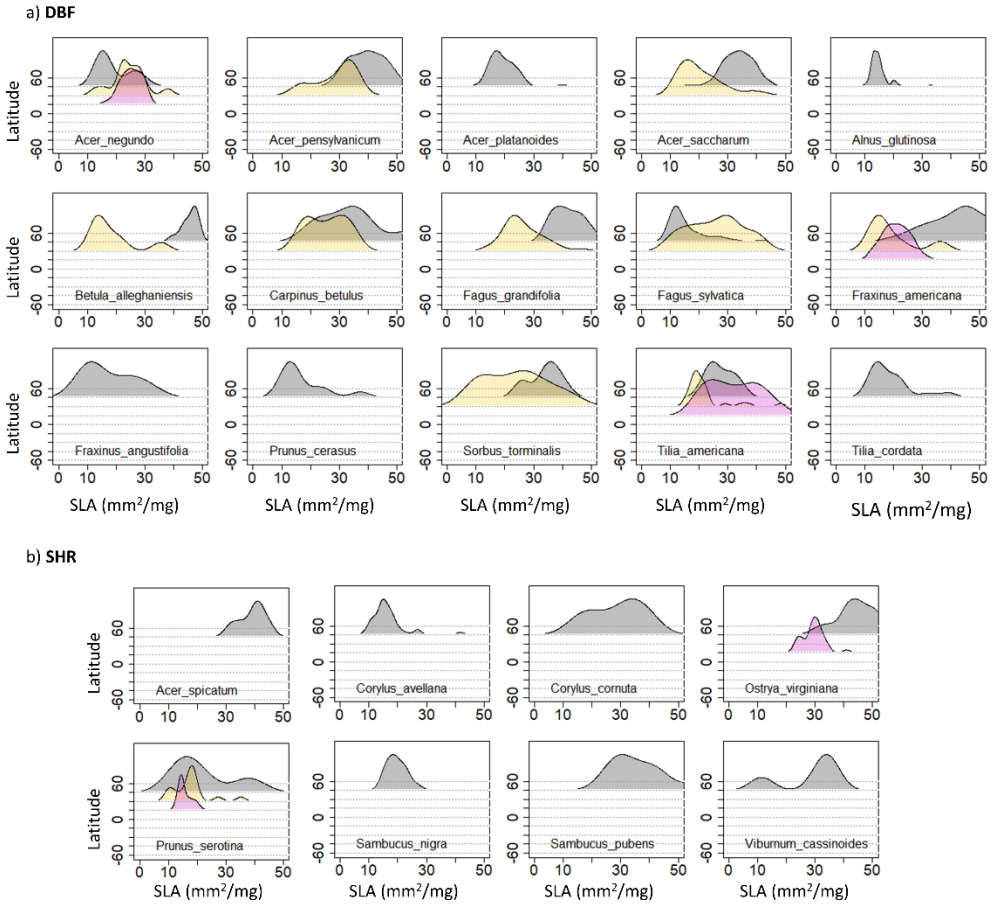

Figure S22: Impact of intra-specific variation on the latitudinal distribution of specific leaf area (SLA). *The data shown is the TRY in-situ data selected by Butler et al. (2017) for the upscaling.*

References

Goll, D.S., Vuichard, N., Maignan, F., Jornet-Puig, A., Sardans, J., Violette, A., Peng, S., Sun, Y., Kvakic, M., Guimberteau, M., 2017. A representation of the phosphorus cycle for ORCHIDEE (revision 4520). Geosci. Model Dev. 10, 3745–3770.

Lang, N., Kalischek, N., Armston, J., Schindler, K., Dubayah, R., Wegner, J.D., 2022. Global canopy height regression and uncertainty estimation from GEDI LIDAR waveforms with deep ensembles. Remote Sens. Environ. 268, 112760. https://doi.org/10.1016/j.rse.2021.112760

Potapov, P., Li, X., Hernandez-Serna, A., Tyukavina, A., Hansen, M.C., Kommareddy, A., Pickens, A., Turubanova, S., Tang, H., Silva, C.E., Armston, J., Dubayah, R., Blair, J.B., Hofton, M., 2021. Mapping global forest canopy height through integration of GEDI and Landsat data. Remote Sens. Environ. 253, 112165. https://doi.org/10.1016/j.rse.2020.112165

Simard, M., Pinto, N., Fisher, J.B., Baccini, A., 2011. Mapping forest canopy height globally with spaceborne lidar. J. Geophys. Res. 116, G04021. https://doi.org/10.1029/2011JG001708

Thum, T., Caldararu, S., Engel, J., Kern, M., Pallandt, M., Schnur, R., Yu, L., Zaehle, S., 2019. A new terrestrial biosphere model with coupled carbon, nitrogen, and phosphorus cycles (QUINCY v1. 0; revision 1772). Geosci. Model Dev. Discuss.

Wang, Y., Li, G., Ding, J., Guo, Z., Tang, S., Wang, C., Huang, Q., Liu, R., Chen, J.M., 2016. A combined GLAS and MODIS estimation of the global distribution of mean forest canopy height. Remote Sens. Environ. 174, 24–43. https://doi.org/10.1016/j.rse.2015.12.005

Zaehle, S., Friend, A.D., 2010. Carbon and nitrogen cycle dynamics in the O-CN land surface model: 1. Model description, site-scale evaluation, and sensitivity to parameter estimates. Glob. Biogeochem. Cycles 24.